ADMLC Webinar: Katabatic Flows

13:00-15:30 GMT Wednesday 13 December 2023

Characteristics of the nocturnal boundary layer using data from the MATERHORN experiment

Silvana Di Sabatino

with contribution by

L. Brogno, F. Barbano, L. S. Leo, H. J. Fernando

Aims of the talk

- Describe some characteristics of the phenomena that characterize the nocturnal boundary-layer over complex terrain
- Focus on the presence of Low-Level jets during the **MATERHORN** field campaign
- Improve the understanding of the double-nosed LLJs **proposing new driving mechanisms for the formation of double-nosed LLJs**

MATERHORN Program

Mountain Terrain Atmospheric Modeling and Observations (2011-2016)

Components:

- MATERHORN-M: Modeling
- MATERHORN-X: Field experiment
- MATERHORN-T: Technology
- MATERHORN-P: Parameterization

Goals: Designed to identify and study the limitations of current state-of-the science meso-scale models for mountain terrain weather prediction and develop new science evidence and tools to help realize leaps in predictability

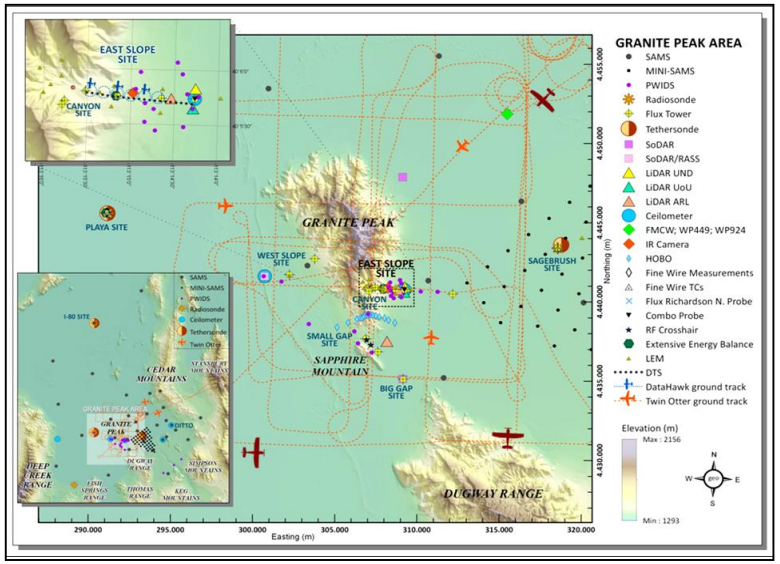

Fernando et al. 2015 – BAMS

MATERHORN Program

AROUND SUNSET

DURING THE NIGHT

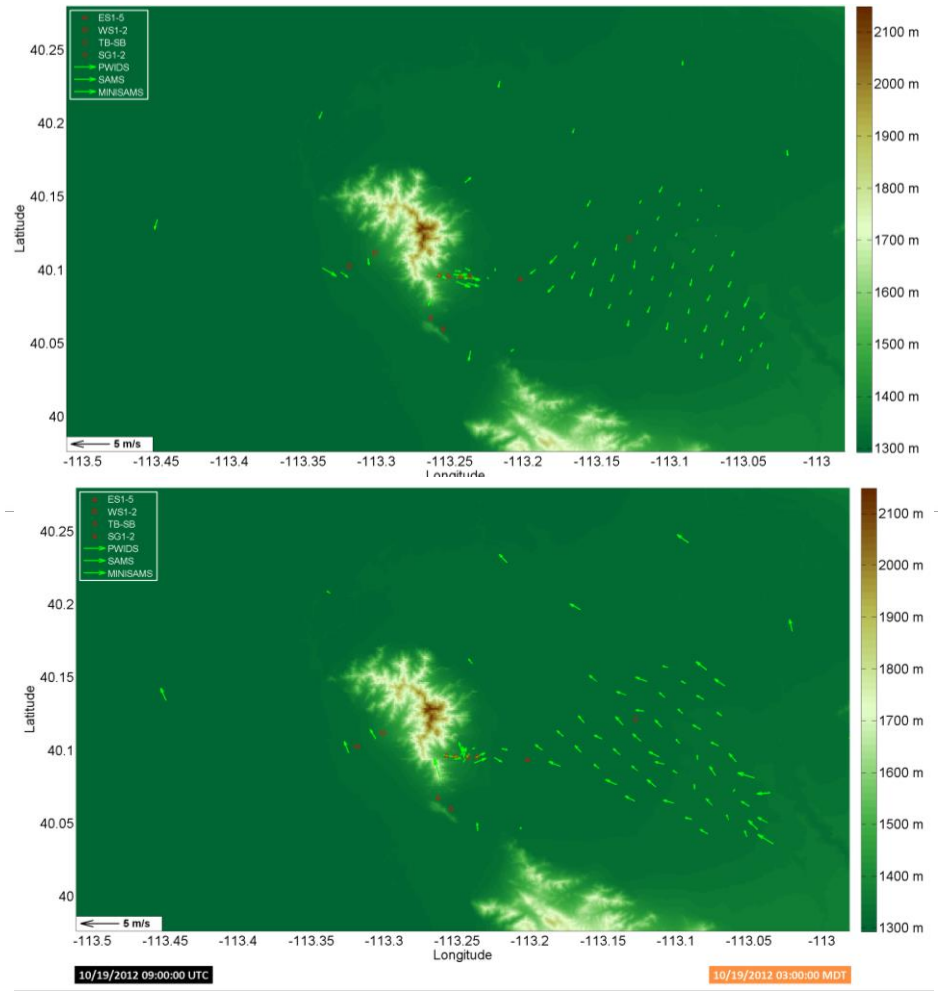

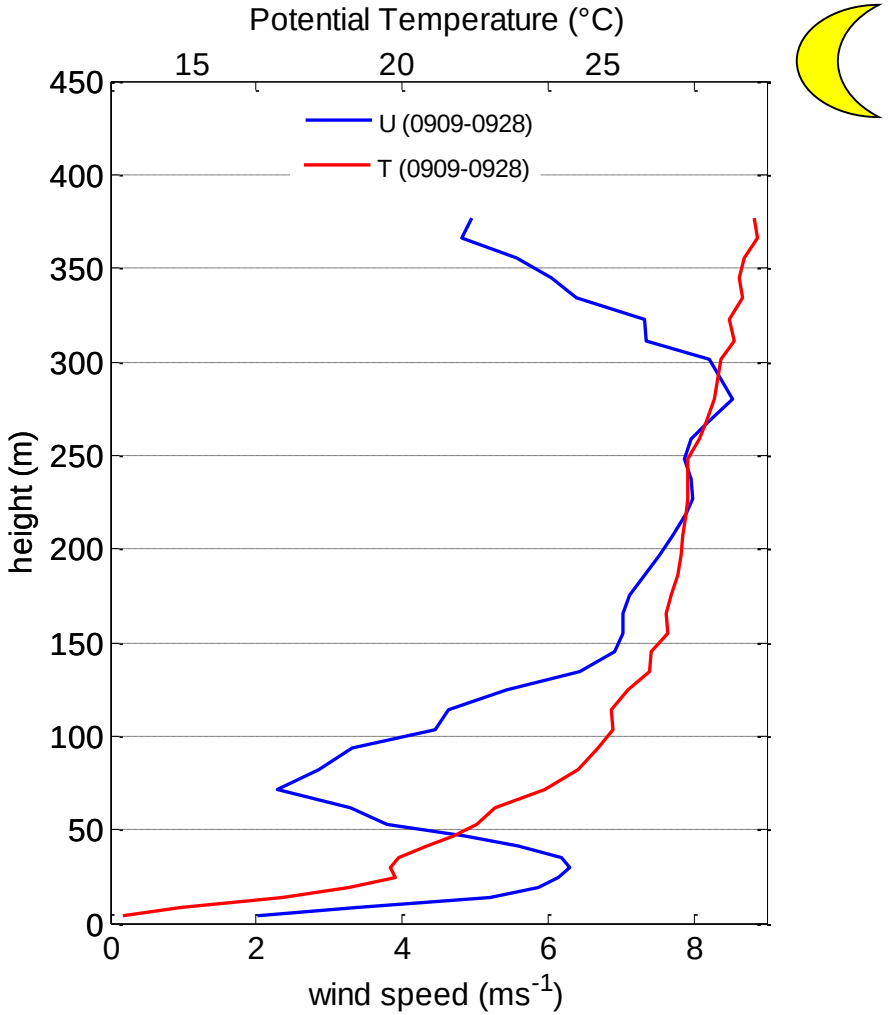

Phenomenology of Low-Level Jet

Low-Level Jet (LLJ) → strong and narrow air stream typically observed within the Planetary Boundary Layer (PBL)

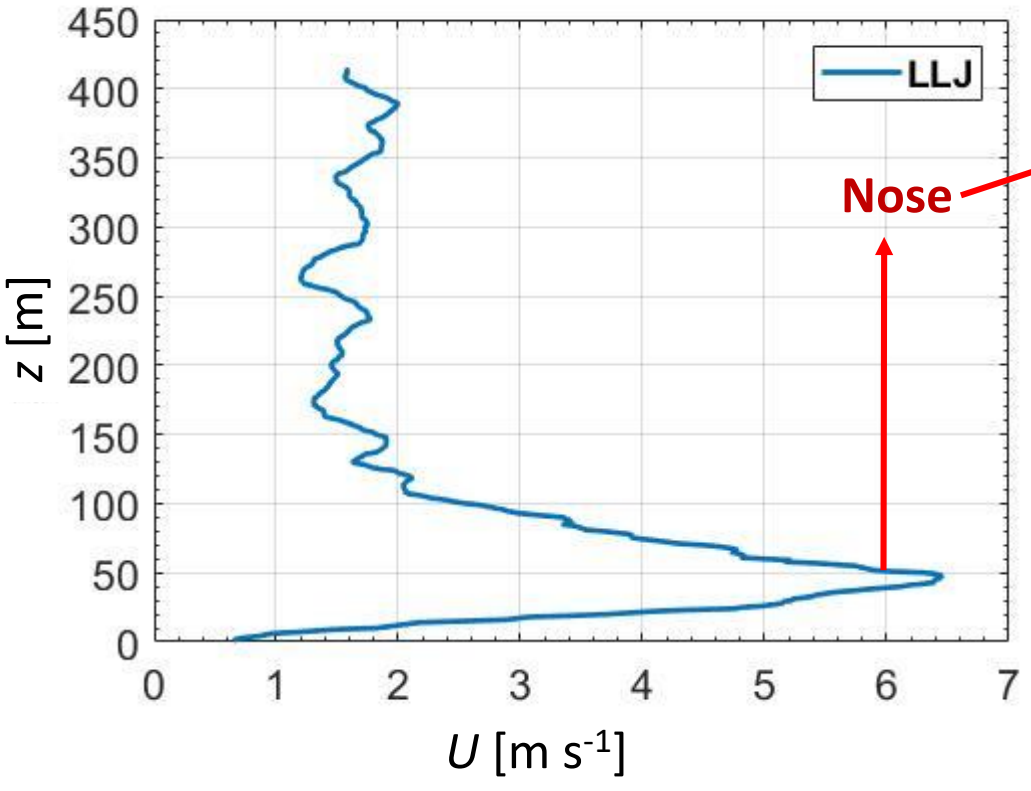

The LLJ wind-speed profile usually takes the shape of a nose, namely **a maximum with a fast decay of the wind speed** with height both below and above it.

Main characteristics:

- **natural atmospheric phenomenon**, mostly investigated on the American Great Plains
- **local feature of the PBL**, not always captured by the mesoscale models
- the spatial scale, the height and the magnitude of the wind-speed maximum **depend on the site and on the driving mechanism**

Phenomenology of Low-Level Jet

Low-Level Jet (LLJ) → strong and narrow air stream typically observed within the Planetary Boundary Layer (PBL)

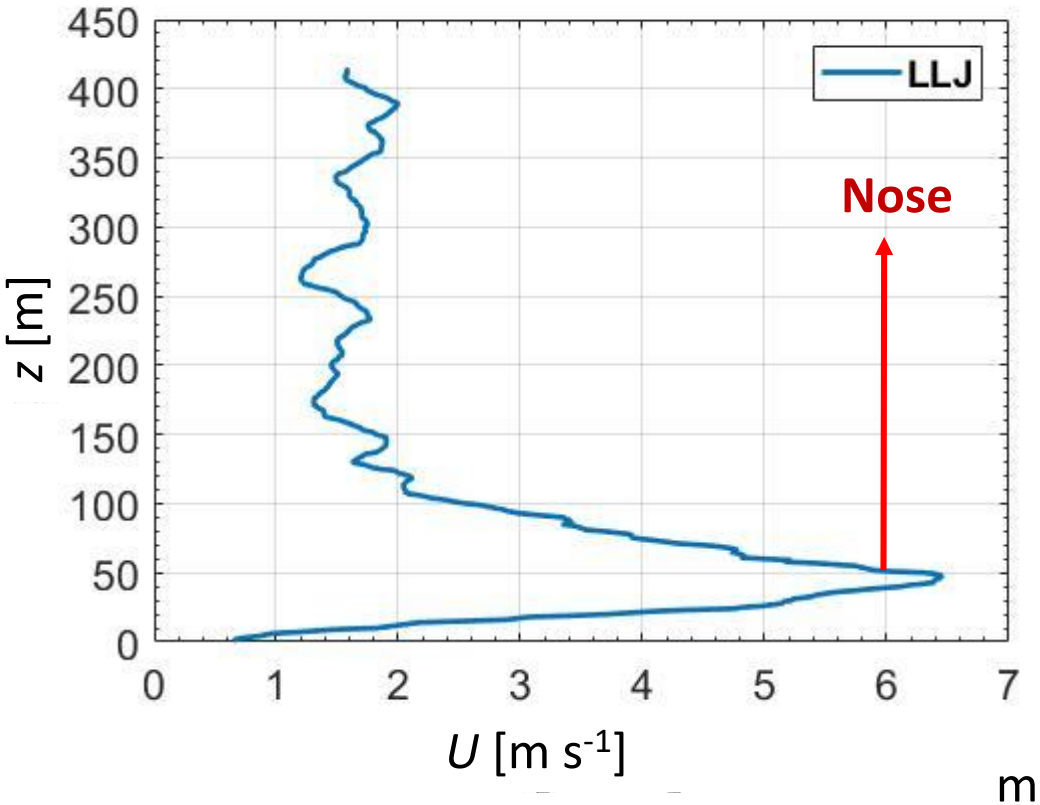

Main driving mechanisms:

- weather patterns at synoptic scale (Wexler, 1961)
- fronts (Droegemeier and Wilhelmson, 1987)
- **mountain and valley winds** (Renfrew and Anderson, 2006)
- **inertial oscillations** (Blackadar, 1957)

↓

undamped oscillations around a nocturnal equilibrium wind vector induced by the Coriolis force

↓

the most frequently observed mechanism under stable stratification

↓

the complex terrain can:

- induce the formation of a LLJ
- interfere with the LLJ dynamics through surface flow perturbation

Phenomenology of Double-Nosed Low-Level Jet

Double-Nosed Low-Level Jet (LLJ) → **simultaneous occurrence of two noses** (i.e. two wind-speed maxima) within the PBL vertical profile of wind speed.

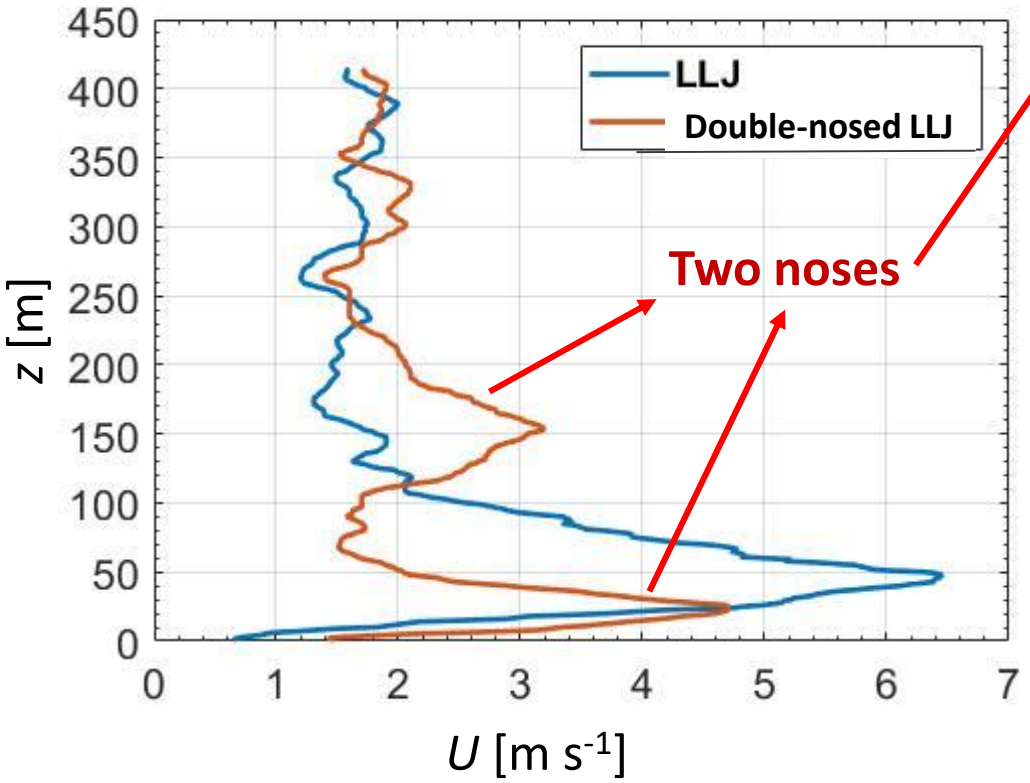

Poorly studied phenomenon:

- **no numerical or analytical studies** of double-nosed LLJs
- observational studies have **not delved into the dynamics and driving mechanisms** of double-nosed LLJs

Few hypotheses of driving mechanisms for double-nosed LLJs, as the one proposed (without validation) by **Banta et al. 2002**

each nose might be driven by **inertial oscillations** associated with horizontal pressure gradients **at different spatial scales**

Site and Dataset selection

The analysed dataset was mainly retrieved at the **Sagebrush site** (red dot) located at the **centre of the Dugway Valley** (Utah, U.S.) during the **MATERHORN** (Mountain Terrain Atmospheric Modeling and Observations) field campaigns

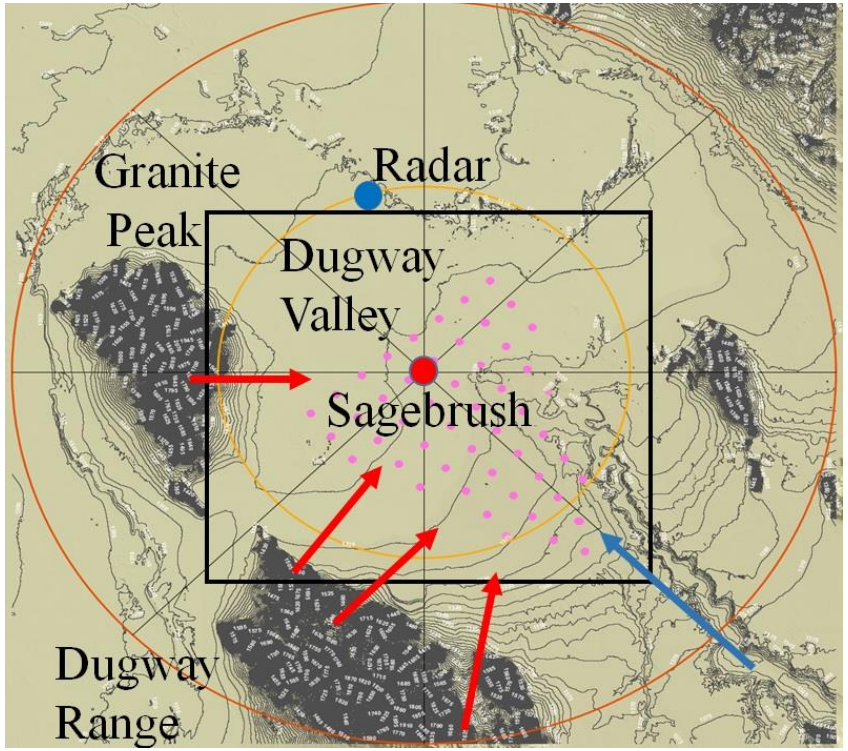

Program aiming at investigating the **complex-terrain meteorology** over a wide range of scales and synoptic conditions (Fernando et al., 2015).

Instrumentation at Sagebrush:

- tethered balloons (Fernando, 2017)
- flux towers (Pace, 2017) equipped with 5 levels (0.5m, 2m, 5m, 10m and 20m) of sonic anemometers coupled with thermohygrometers.

Other Instrumentation: standard weather stations (pink dots, Pace, 2016)

Site and Dataset selection

Only **quiescent Intensive Observing Periods (IOPs)** were analysed (when $U < 5\ ms^{-1}$, in which U is the 700 hPa wind speed, Fernando et al. 2015)

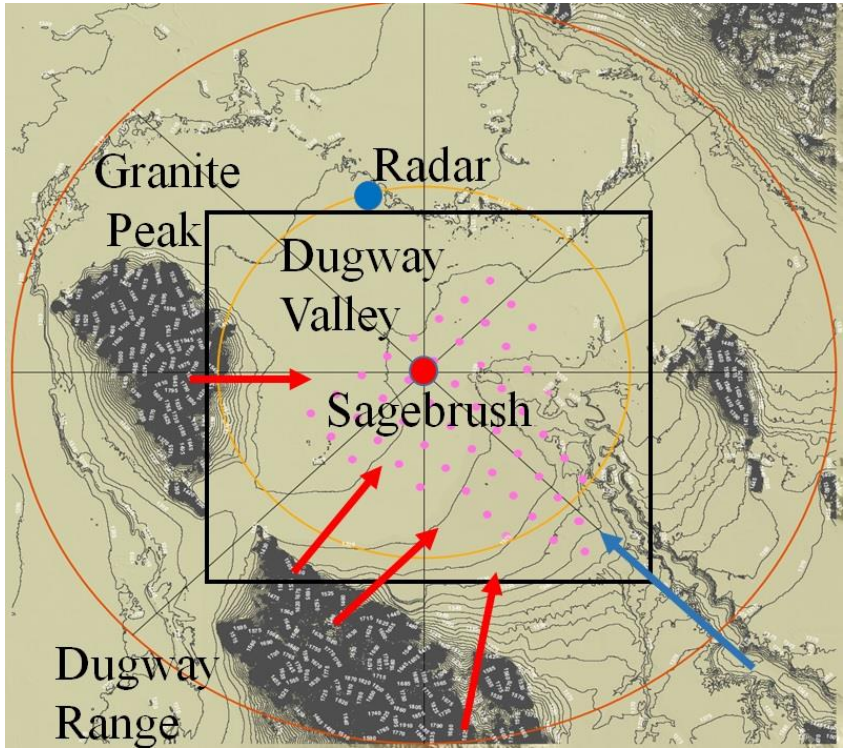

the **weak synoptic forcing** did not alter the boundary-layer dynamics

Quiescent IOPs

		Operational period
Fall 2012	IOP0	2000 UTC 25/09 – 2000 UTC 26/09
	IOP1	2000 UTC 28/09 – 2000 UTC 29/09
	IOP2	2000 UTC 01/10 – 2000 UTC 02/10
	IOP6	0800 UTC 14/10 – 0800 UTC 15/10
	IOP8	1100 UTC 18/10 – 1800 UTC 19/10
Spring 2013	IOP4	2000 UTC 11/05 – 2000 UTC 12/05
	IOP7	2315 UTC 20/05 – 2000 UTC 21/05

Local time MDT = UTC - 6 h

Flow characteristics:

- **downvalley flow** (SE-NW, blue line)
- development of a **LLJ** along the main valley axis (SE-NW, blue line)
- **flow perturbations** as downslope flows from the surrounding mountains may **intrude the valley and trigger the generation of waves**

Nocturnal Evolution of the Wind Speed

We observed the nocturnal evolution of the main atmospheric variables to understand the LLJ driving mechanisms.

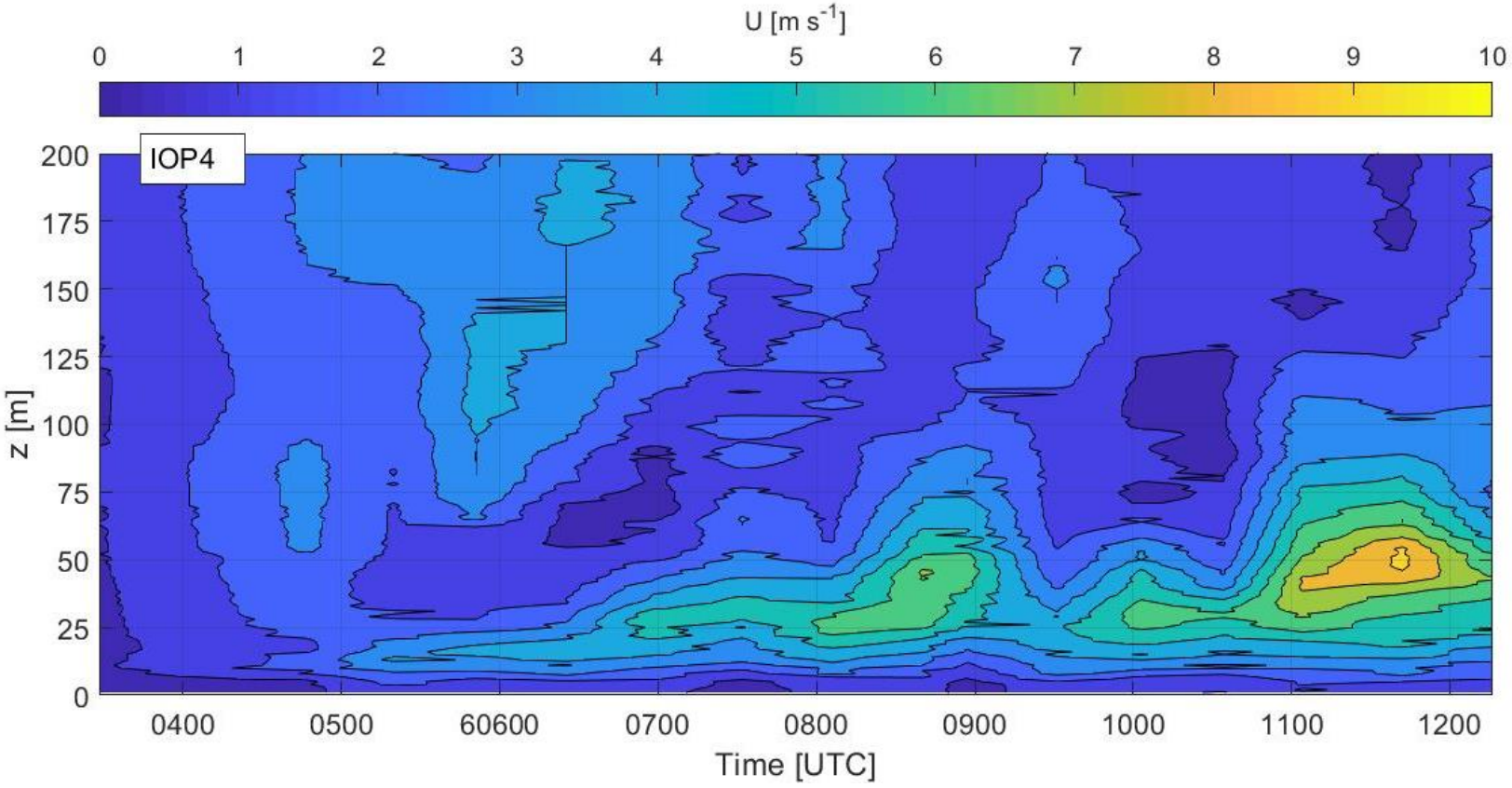

IOP4

Sunset 0233 UTC

Sunrise 1214 UTC

Local time MDT = UTC - 6 h

- The LLJ dynamics starts during the first hours of night
- The magnitude of the LLJ wind-speed maximum increases during the night until sunrise
- The LLJ wind-speed maximum is between 20 m and 60 m AGL

Nocturnal Evolution of the Wind Direction

We observed the nocturnal evolution of the main atmospheric variables to understand the LLJ driving mechanisms.

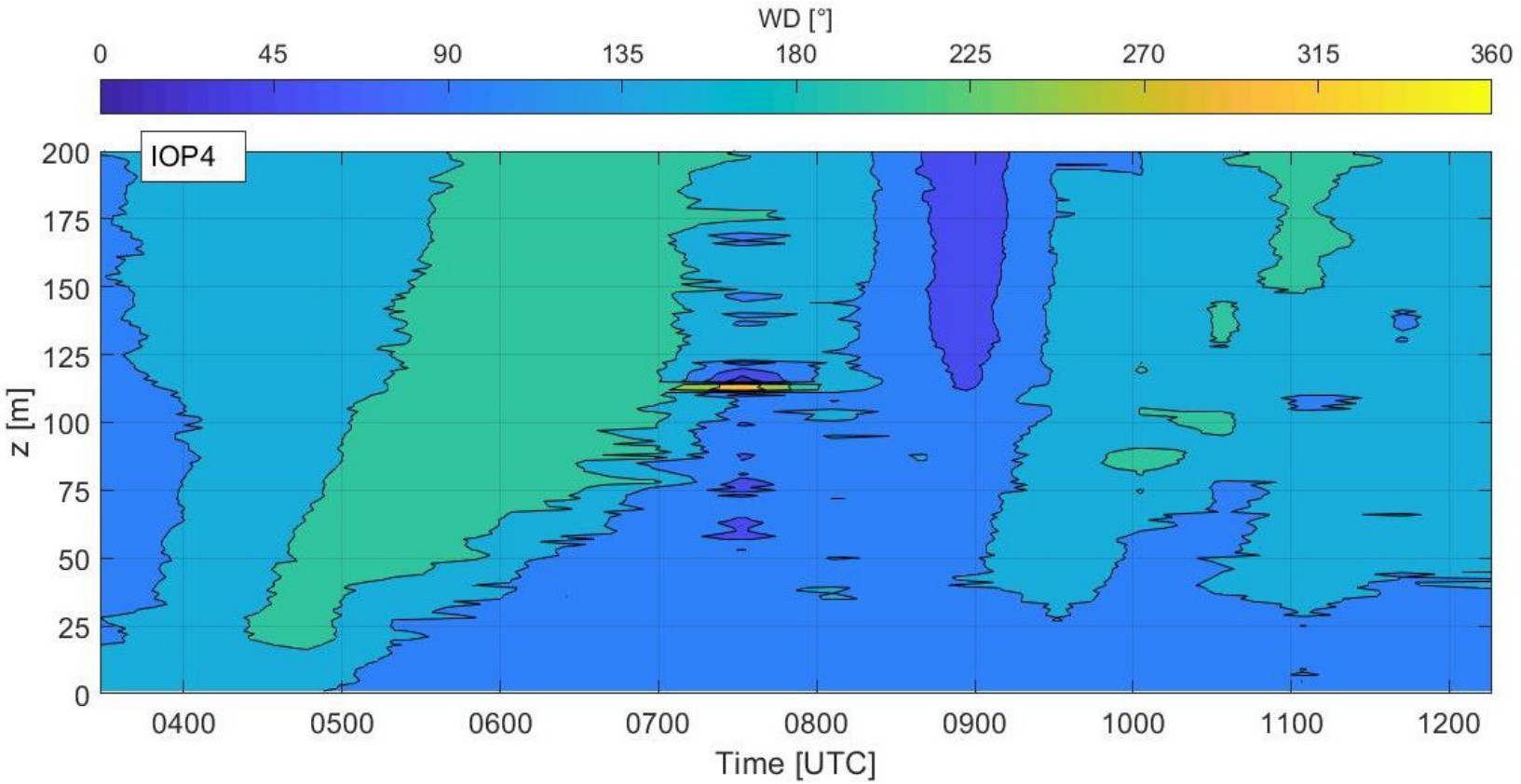

IOP4

Sunset 0233 UTC

Sunrise 1214 UTC

Local time MDT = UTC - 6 h

- LLJ dynamics starts at the onset of the downvalley flow (i.e. the LLJ is along the main valley axis, SE-NW)

Nocturnal Evolution of the Potential Temperature

We observed the nocturnal evolution of the main atmospheric variables to understand the LLJ driving mechanisms.

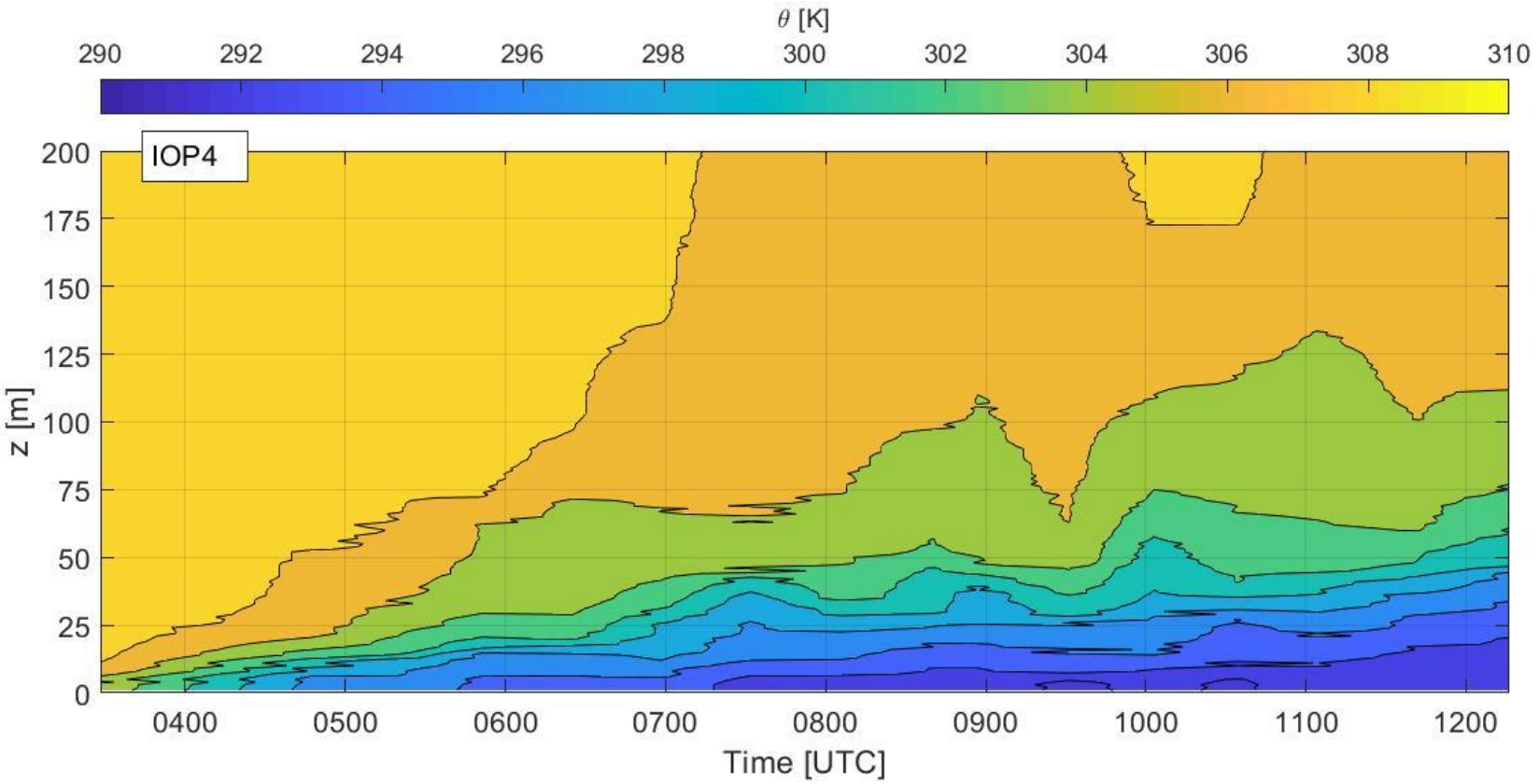

IOP4

Sunset 0233 UTC

Sunrise 1214 UTC

Local time MDT = UTC - 6 h

- Development of a stable stratification during the night

Low-Level Jet Evolution

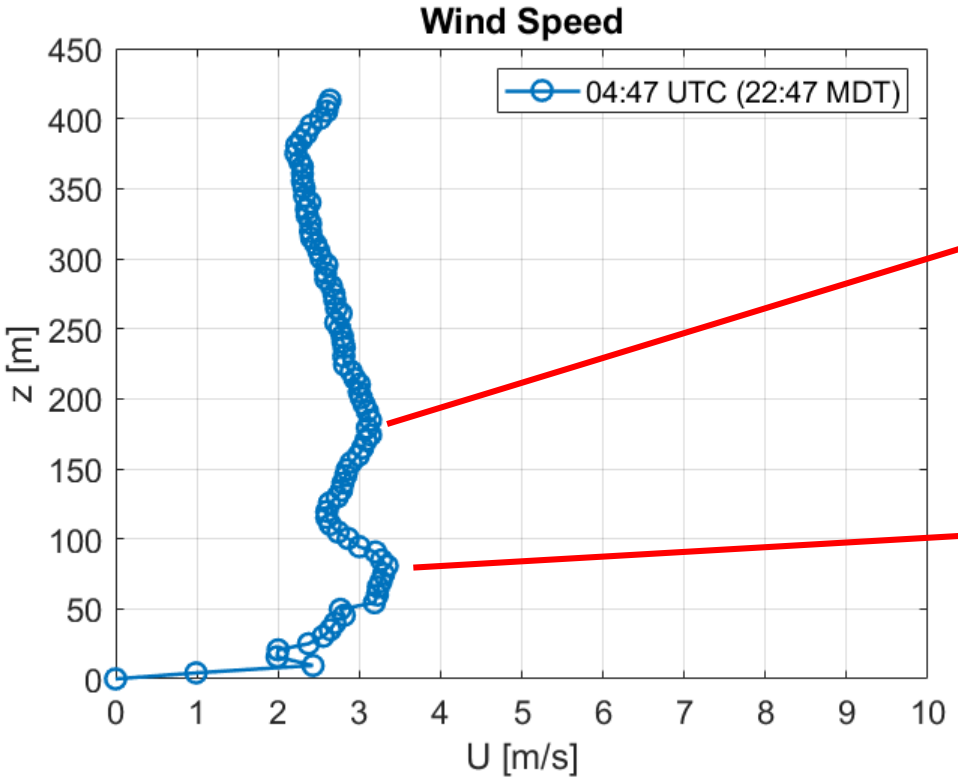

During the early night, the wind speed profile is **homogeneous**

A **local velocity maximum** starts to grow at the surface, confined by the residual layer

Initial profile

| t

Low-Level Jet Evolution

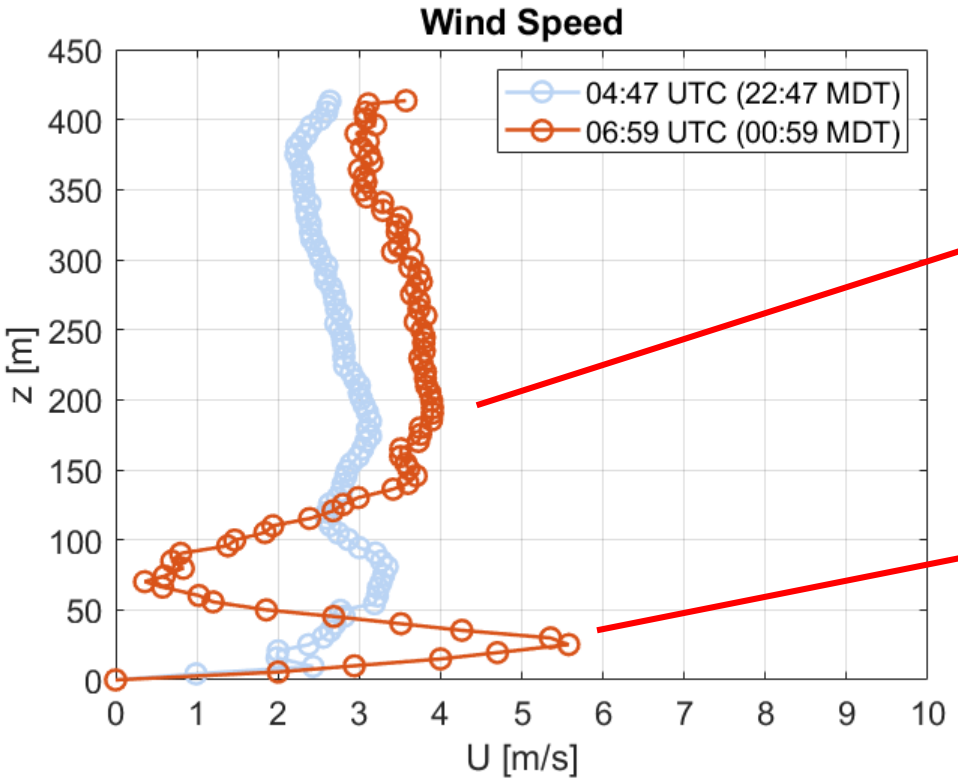

The depth of the residual layer is decreasing while it is perturbed by the basin flow

A wind speed maximum rises in the stable layer at the surface: a low-level jet is formed

Low-Level Jet Evolution

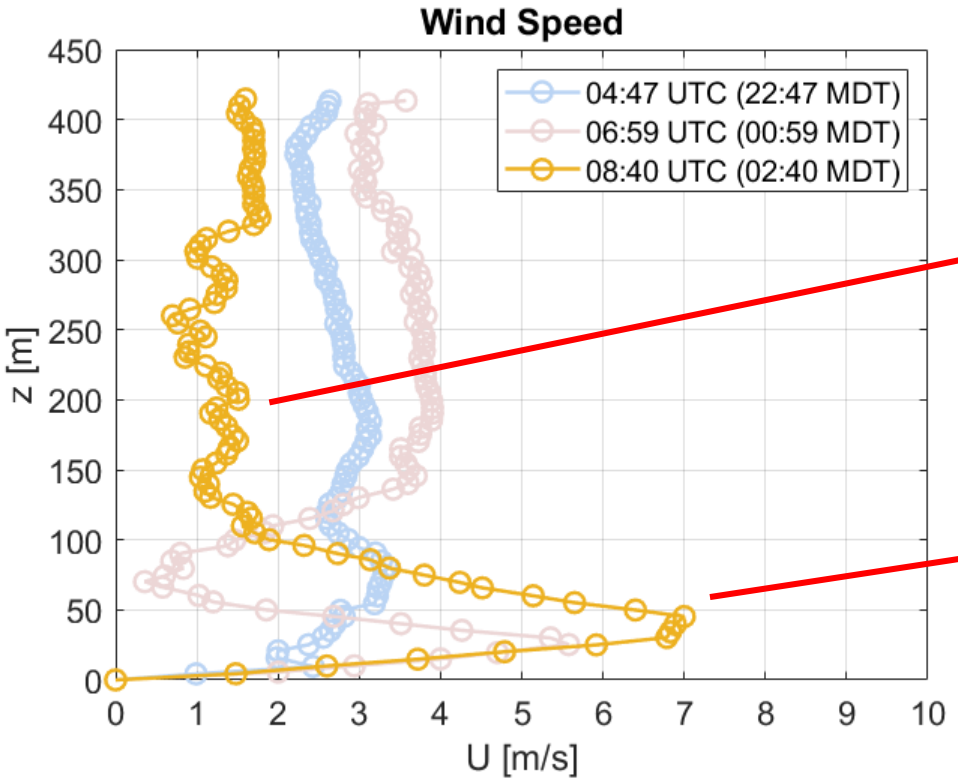

Wind speed in the residual layer rapidly decreases as the stable layer cut off the energy and momentum vertically transported from the surface

The **low-level jet grows** in **magnitude** and **depth**

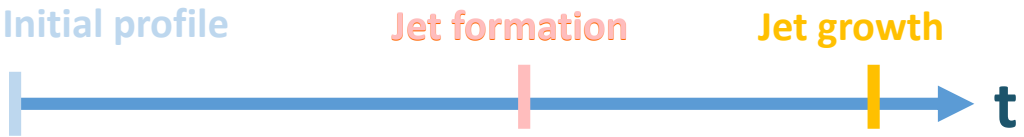

Low-Level Jet Evolution

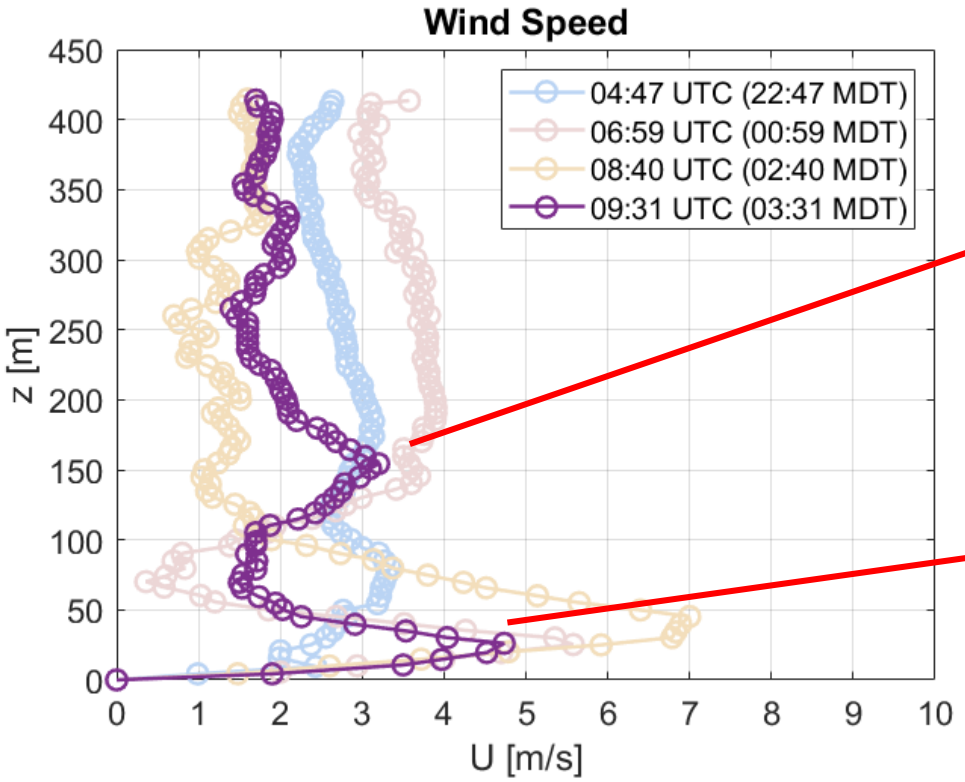

The anomalous behavior gives birth to a **secondary wind speed maximum**: the profile evolves in a **double-nosed LLJ**

The **low-level jet is perturbed**, resulting in a **sudden decrease of wind speed** and **jet depth**

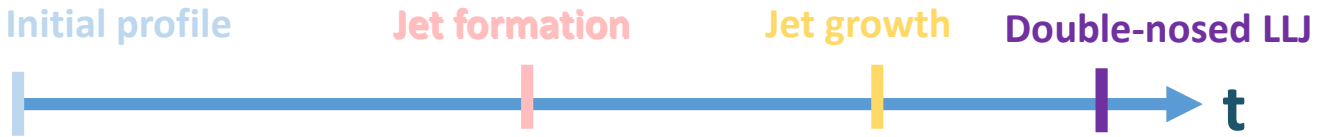

Low-Level Jet Evolution

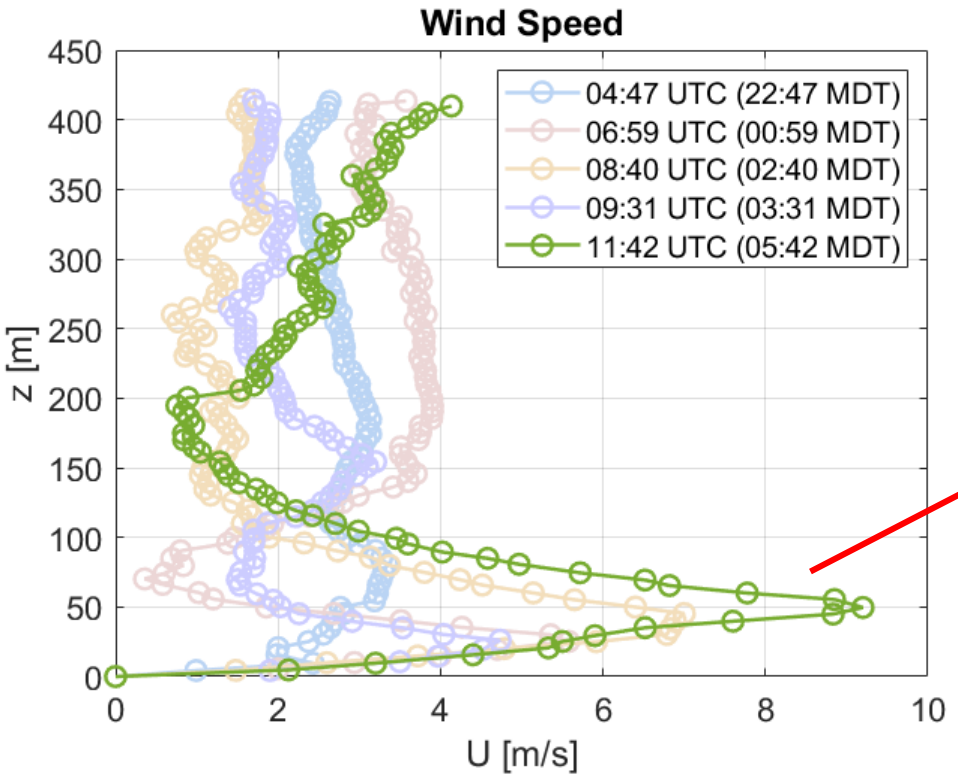

As the anomaly is restored to the common **single-maximum shape**, the **low-level jet continues to grow** reaching its **full development** both in wind speed and jet depth

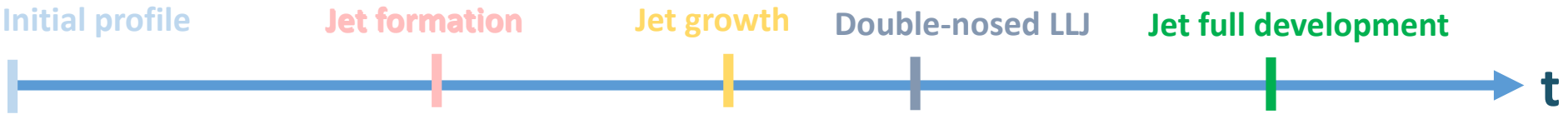

Low-Level Jet Evolution

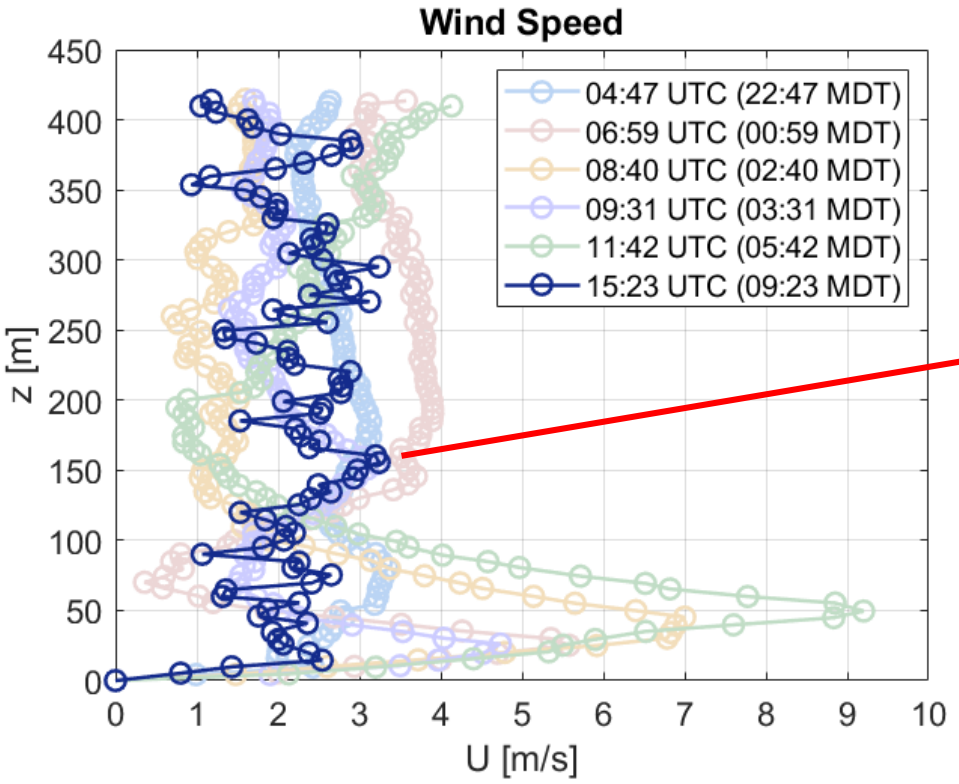

After few hours from the sunrise, the **low-level jet completely replaced by the diurnal flow**

Nocturnal Evolution

- The nocturnal evolution of the wind speed and direction suggest the **thermal circulation drives the early-evening development** of the LLJ while being progressively superimposed by **the inertial oscillations that regulate the subsequent nocturnal evolution** of the LLJ up to the sunrise.

What are the main mechanisms of formation of the double-nosed LLJS?

Driving Mechanisms for Double-nosed LLJ

20 double-nose LLJs are classified considering two newly-proposed driving mechanisms:

- **wind-driven mechanism**
  (15 double-nose LLJs)
  - the two noses are associated with **different air masses flowing one on top of the other.**
  - sharp and pronounced variation of the wind-direction between the primary and the secondary nose.
- **wave-driven mechanism**
  (5 double-nose LLJs)
  - a flow perturbation generates a wave. This **wave vertically transports momentum causing the occurrence of a secondary nose**, leading to the formation of a double-nosed LLJ
  - small and nearly constant rotation with the height within the PBL

The necessary conditions to observe such mechanisms are: (i) the presence of a **weak-synoptic forcing**, not altering the boundary-layer dynamics; (ii) the existence of an **already-established LLJ**, (iii) the occurrence of a **local flow perturbation** and (iv) the development of a **local wave capable of vertically transporting the flow momentum** (pre-requisite of one mechanism only).

Driving Mechanisms for Double-nosed LLJ

20 double-nose LLJs are classified considering two newly-proposed driving mechanisms:

- **wind-driven mechanism**

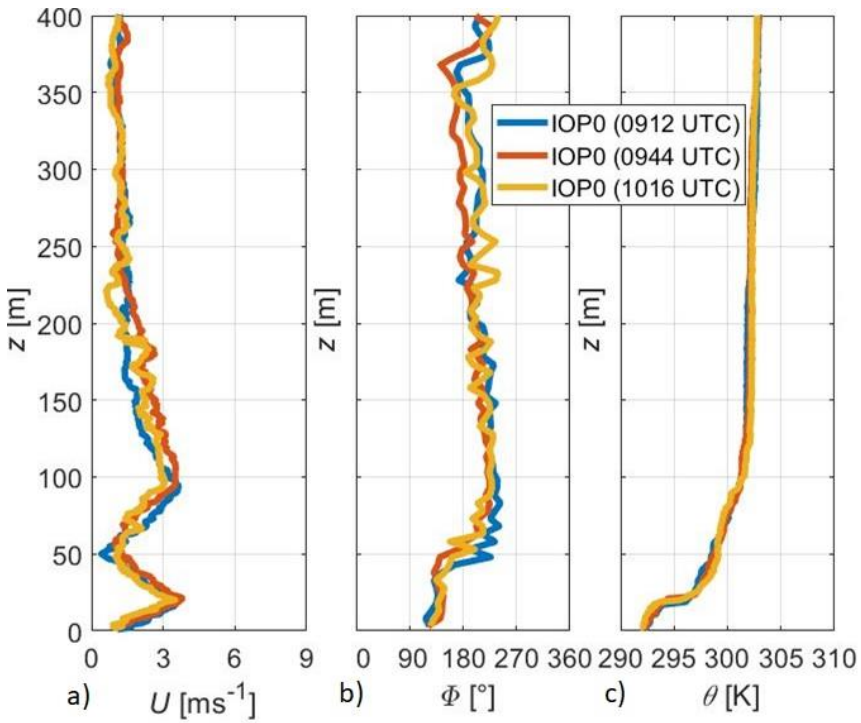

- **wave-driven mechanism**

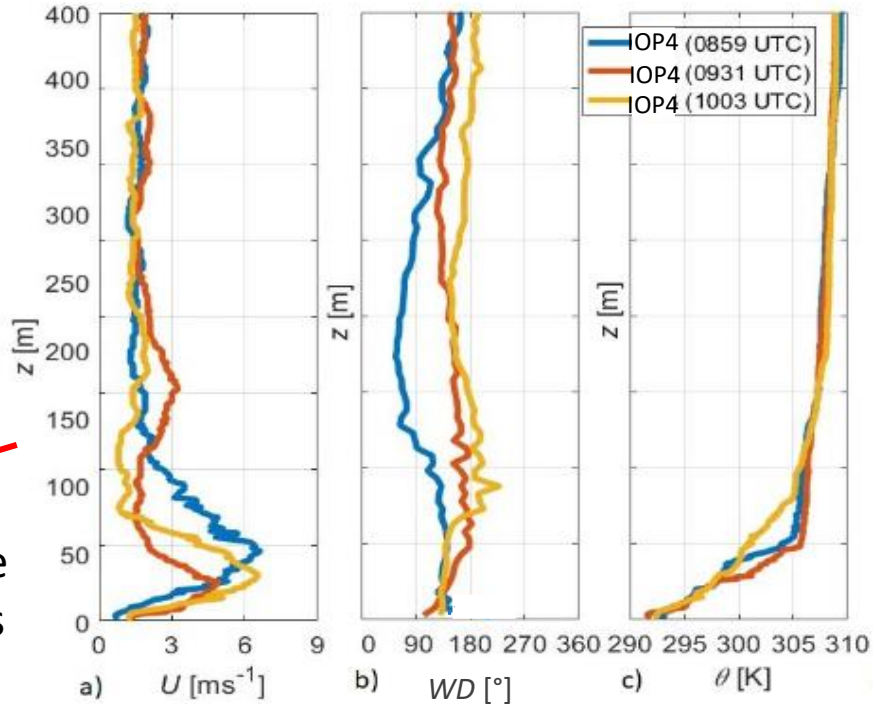

notice that only the profile at 0931 UTC is classified as double-nosed LLJ

Wave-Driven Mechanism

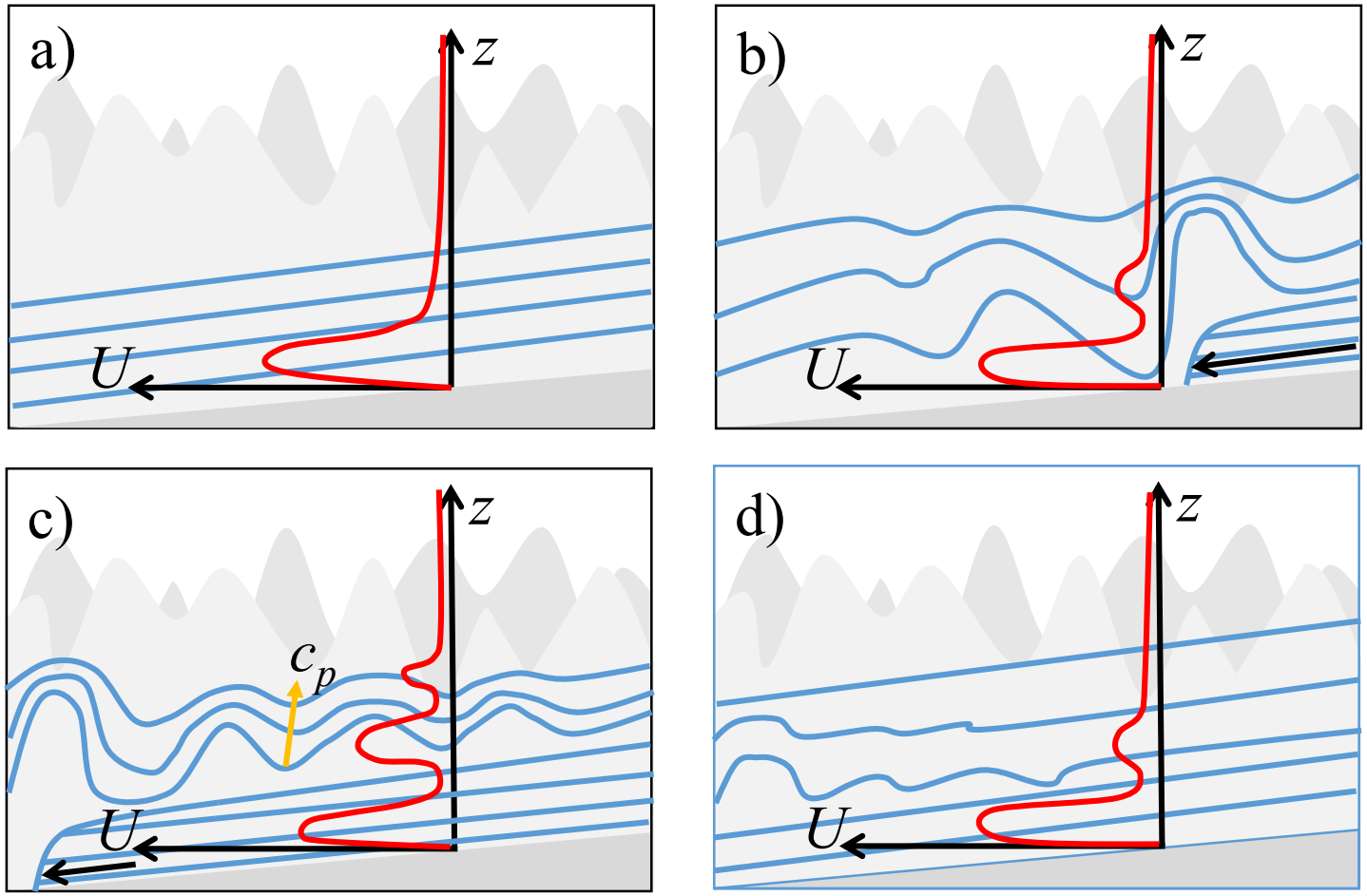

Phases of the wave-driven mechanism:

(a) already-established LLJ

(b) wave generation triggered by a flow perturbation

(c) secondary nose formation

(d) dissipation (if the wave is dispersive)

The blue lines represent hypothetical streamlines of wind speed, the red lines the wind-speed profile, the yellow arrow the phase velocity of the wave c_p, the grey triangles a generic sloping terrain and the grey shading in the background the surrounding topography

Brogno et al 2021, JAS 78(12)

Wave-Driven Mechanism

Flow perturbation → Wave generation → Vertical momentum transport → Double-nosed LLJ → Dissipation

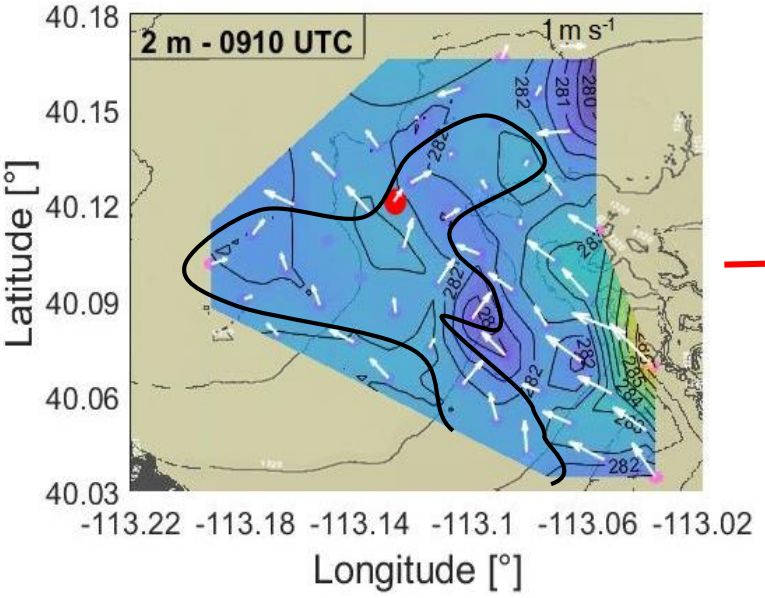

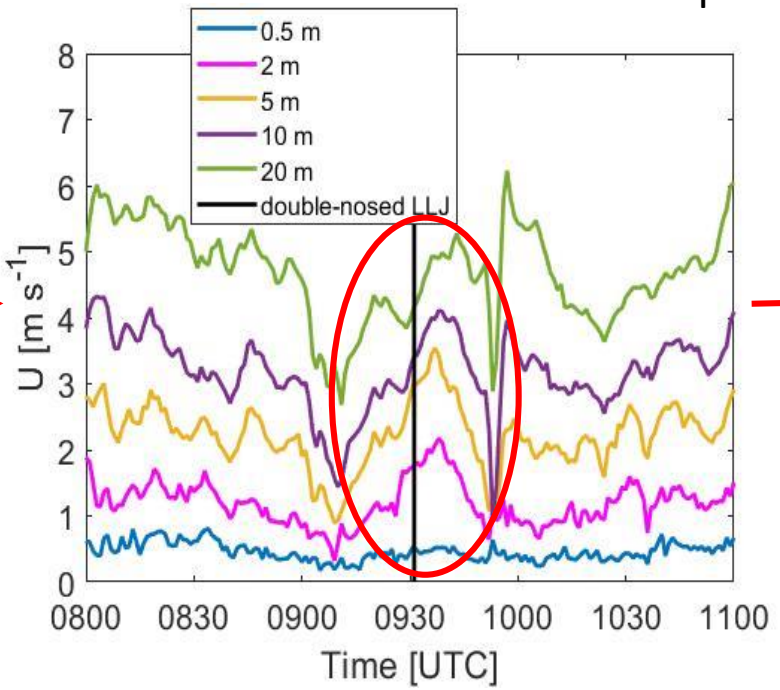

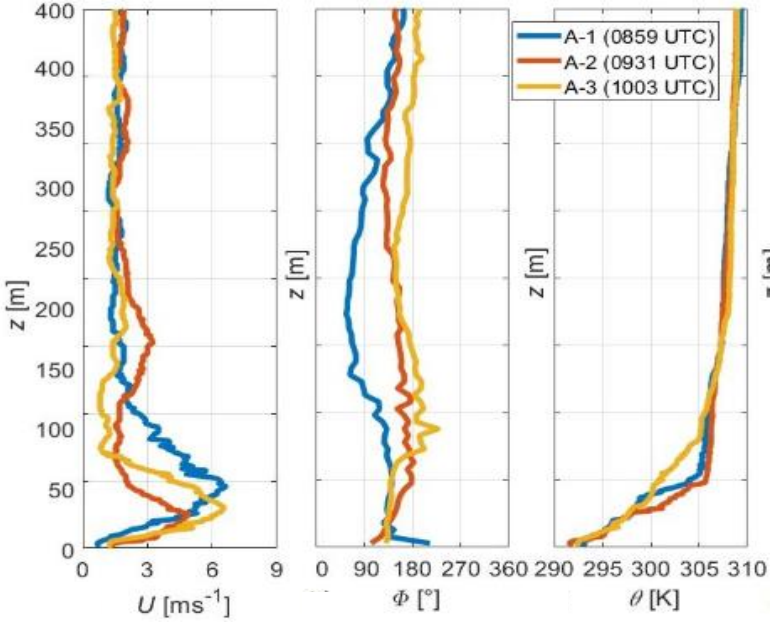

Inertial-gravity wave dispersion relation:

$$\omega^2 = \frac{k_z^2 f^2 + k_H^2 N^2}{K^2} \rightarrow \omega^2 = f^2 sin^2\,\phi + N^2\,cos^2\,\phi$$

$$K = \sqrt{k_x^2 + k_y^2 + k_z^2}$$

$$k_H = \sqrt{k_x^2 + k_y^2}$$

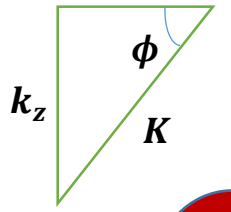

Wave-Driven Mechanism: Vertical Momentum Transport

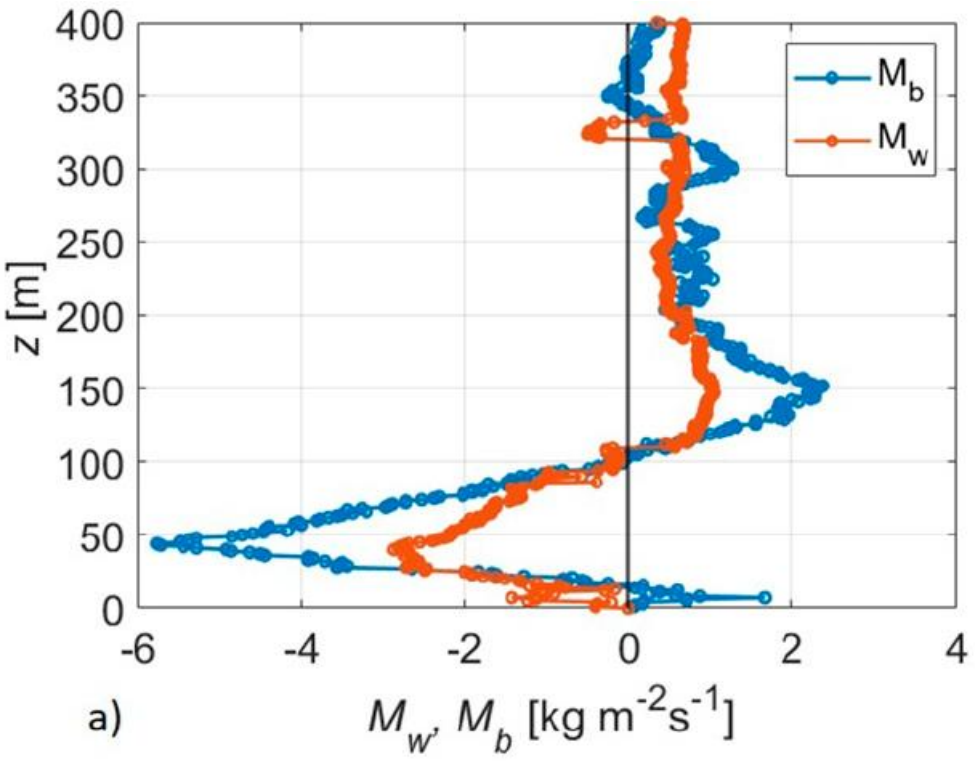

The vertical momentum transport due to an inertial-gravity wave was verified by two methods:

- **as proposed in literature (Kim and Mahrt, 1992)**

$$M_w(z) = \rho(z)\sqrt{\frac{\left(\overline{\tilde{w}\tilde{u}}(z), \overline{\tilde{w}\tilde{v}}(z)\right) \cdot (u(z), v(z))}{U(z)}}$$

- **with a bulk estimation**

$$M_b(z) = \rho_2(z)U_2(z) - \rho_1(z)U_1(z)$$

ρ air density,
$\overline{\tilde{w}\tilde{u}}$ and $\overline{\tilde{w}\tilde{v}}$ streamwise and cross-stream wave momentum fluxes,
$U = \sqrt{u^2 + v^2}$ the wind-speed intensity,
Z depth of the atmospheric layer involved in the momentum transport,
subscript 1= closest profile prior to the double-nosed LLJ,
subscript 2= double-nosed LLJ profile

Wave-Driven Mechanism: Vertical Momentum Transport

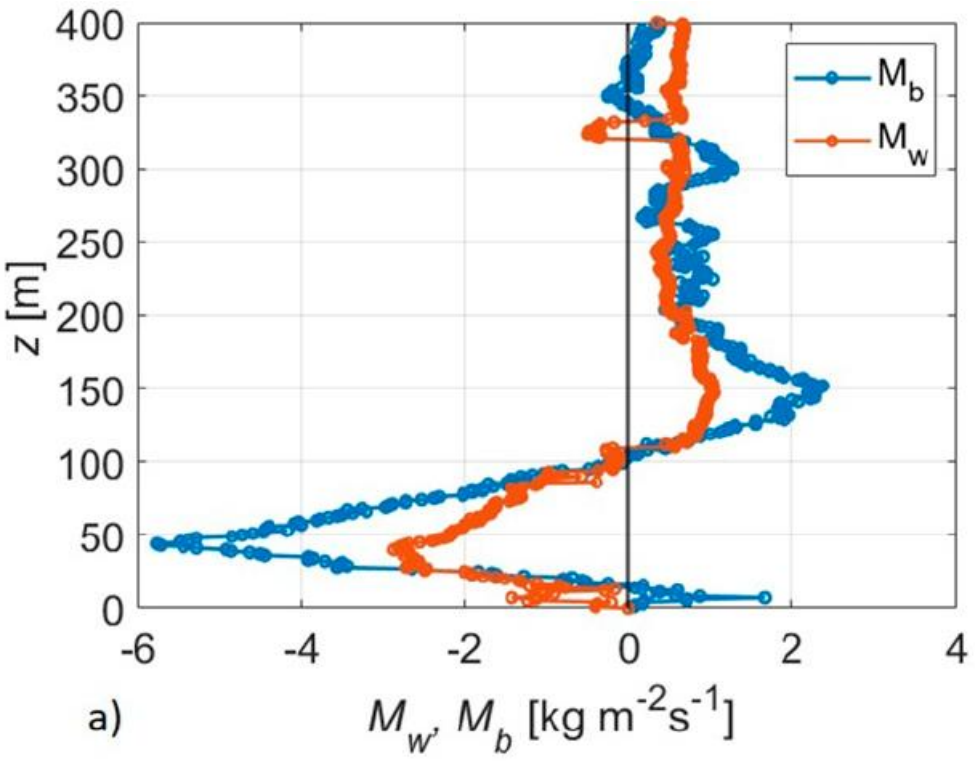

Comparison between the **mean wave momentum loss by the primary nose** (0-100 m) and **mean wave momentum gain by the secondary nose** (100-250 m):

$$M_w^{loss} \approx -1.44\ \mathrm{kg}\, m^{-2} s^{-1} \text{ from } z_i = 0\ m \text{ to } z_f = 100\ m,$$

$$M_w^{gain} \approx 0.82\ \mathrm{kg}\, m^{-2} s^{-1} \text{ from } z_i = 100\ m \text{ to } z_f = 250\ m,$$

$$\frac{M_w^{gain}}{M_w^{loss}} \approx 57\%$$

$$M_b^{loss} \approx -2.01\ \mathrm{kg}\, m^{-2} s^{-1} \text{ from } z_i = 0\ m \text{ to } z_f = 100\ m,$$

$$M_b^{gain} \approx 1.21\ \mathrm{kg}\, m^{-2} s^{-1} \text{ from } z_i = 100\ m \text{ to } z_f = 250\ m,$$

$$\frac{M_b^{gain}}{M_b^{loss}} \approx 60\%$$

The remaining 40-43% may be dissipated by the wave, strengthening the effect of a dispersive wave as a momentum carrier.

Conclusions

- During MATERHORN, the **thermal circulation drives the early-evening development** of the LLJ while being progressively superimposed by **the inertial oscillations that regulate the subsequent nocturnal evolution** of the LLJ up to the sunrise.

- **20 double-nosed LLJs** (the **19%** of the total number of nocturnal tethered-balloon profiles) were identified using **refined criteria** proposed in the literature.

- **Two new driving mechanisms** of double-nosed LLJs are proposed:

  - the **wind-driven mechanism** which describes noses associated with different air masses simultaneously flowing one above the other from different directions.

  - the **wave-driven mechanism** which assumes that the secondary-nose formation is driven by the vertical momentum transport carried by a wave, the latter being caused by an external flow perturbation.

References

- Baas, P., F. C. Bosveld, H. K. Baltink, and A. A. M. Holtslag, 2009: A climatology of Nocturnal Low-Level Jets at Cabauw. J. Appl. Meteor. Climatol.,48 (8), 1627–1642, doi:10.1175/2009JAMC1965.1
- Banta, R. M., R. K. Newsom, J. K. Lundquist, Y. L. Pichugina, R. L. Coulter, and L. Mahrt, 2002: Nocturnal Low-Level Jet Characteristic over Kansas During CASES-99.Boundary-Layer Meteor.,105 (2), 221–252, doi:10.1023/A:1019992330866
- Barbano, F., Leo, L. S., Brogno, L., & Di Sabatino, S. (in preparation). Double-nosed Low-Level Jet in Complex Terrain: a model from Inertial Oscillations
- Blackadar A. K., 1957: Boundary Layer Wind Maxima and Their Significance for the Growth of Nocturnal Inversions. Bull. Amer. Meteor. Soc., 38(5), 283–290, doi:10.1175/1520-0477-38.5.283
- Brogno, L., Barbano, F., Leo, L. S., Fernando, H. J., & Di Sabatino, S., 2021: Driving mechanisms of double-nosed low-level jets during materhorn experiment. *Journal of the Atmospheric Sciences*, *78*(12), 4037-4051, doi: 10.1175/JAS-D-20-0274.1
- Droegemeier, K. K., Wilhelmson, R. B., 1987: Numerical Simulation of Thunderstorm Outflow Dynamics. Part I: Outflow Sensitivity Experiments and Turbulence Dynamics. J. Atmos. Sci., 44(8), 1180–1210, doi:10.1175/1520-0469(1987)044<1180:NSOTOD>2.0.CO;2
- Fernando, H., 2017: Vaisala DigiCORA Tethersonde System Data Sage Brush Site. Version 1.0. UCAR/NCAR - Earth Observing Laboratory. Accessed 18 Apr 2020.
- Fernando, H. J. S., and Coauthors, 2015: The MATERHORN Unraveling the Intricacies of Mountain Weather. Bull. Amer. Meteor. Soc.,96 (11), 1945–1967, doi:10.1175/BAMS-D-13-00131.1

References

- Kim, J., and L. Mahrt, 1992: Momentum Transport by Gravity Waves. J. Atmos. Sci.,49 (9), 735–748
- Pace, J., E. Pardyjak, and H. Fernando, 2017: MATERHORN-X Tower Data. Version 1.0. UCAR/NCAR - Earth Observing Laboratory. Accessed 18 Apr 2020.
- Pace, J., 2016: Surface Atmospheric Measurement Stations Mini Network 1 Minute Average Data located to East and South East of granite Peak. Version 1.0.UCAR/NCAR - Earth Observing Laboratory. Accessed 18 Apr 2020
- Renfrew, I. A., Anderson, P. S., 2006: Profiles of katabatic flow in summer and winter over Coats Land, Antarctica. Q. J. R. Meteor. Soc., 132(616), 779–802, doi: 10.1256/qj.05.148
- Shapiro. A., Fedorovich, E., 2009: Nocturnal low-level jet over a shallow slope. Acta Geophys., 57(4). 950–980, doi:10.2478/s11600-009-0026-5
- Van De Wiel, B. J. H., A. F. Moene, G. J. Steeneveld, P. Baas, F. C. Bosveld, and A. A. M. Holtslag, 2010: A conceptual view on inertial oscillations and nocturnal low-level jets. J. Atmos. Sci., 67 (8), 2679–2689, doi:10.1175/2010JAS3289.1
- Wexler, H., 1961: A Boundary Layer Interpretation of the Low-level Jet. Tellus, 13(3), 369–378, doi:10.1111/j.2153-3490.1961.tb00098.x


Thank you very much for your attention!